Diethylenetriamine-functionalized chitosan magnetic nano-based particles for the sorption of rare earth metal ions [Nd(III), Dy(III) and Yb(III)]

Ahmed A. Galhoum, Mohammad G. Mahfouz, Sayed T. Abdel-Rehem, Nabawia A. Gomaa, Asem A. Atia, Thierry Vincent, Eric Guibal

Diethylenetriamine-functionalized chitosan magnetic nano-based particles for the sorption of rare earth metal ions [Nd(III), Dy(III) and Yb(III)]

Ahmed A. Galhoum · Mohammad G. Mahfouz · Sayed T. Abdel-Rehem · Nabawia A. Gomaa · Asem A. Atia · Thierry Vincent · Eric Guibal

Abstract The recovery of three rare earth (RE) metals ions [Yb(III), Dy(III) and Nd(III), belonging to heavy, mild and light REs, respectively] was investigated using hybrid chitosan-magnetic nano-based particles functionalized by diethylenetriamine (DETA). The effect of pH on sorption performance was analyzed: the optimum initial pH value was found close to 5 (equilibrium pH value close to 6.5). The nanometric size of sorbent particles (30–50 nm) minimized the contribution of resistance to intraparticle diffusion on the control of uptake kinetics, which is efficiently modeled using the pseudo-second order rate equation: under selected experimental conditions the contact time required for reaching equilibrium was less than 1 h. Sorption isotherms were efficiently modeled using the Langmuir equation: maximum sorption capacities reached about 50 mg metal g^{-1}, regardless of the RE. The temperature had a very limited effect on sorption capacity (in the range 300–320 K). The thermodynamic parameters were determined: the sorption was endothermic (positive values of $\Delta H°$), spontaneous (negative values of $\Delta G°$) and contributed to increasing the disorder of the system (positive values of $\Delta S°$). The three REs have similar sorption properties on DETA-functionalized chitosan magnetic nano-based particles: the selective separation of these elements seems to be difficult. The sorbed metal ions can be removed from loaded sorbents using thiourea, and the sorbent can be recycled for at least five sorption/desorption cycles with a limited loss in sorption performance (by less than 6 %). The saturation magnetization was close to 20 emu g^{-1}; this means that nano-based superparamagnetic particles can be readily recovered by an external magnetic field, making the processing of these materials easy.

Keywords Sorption isotherms · Uptake kinetics · Sorbent recycling · Rare earth metal ions · Chemically modified chitosan · Magnetic nano-based particles

A. A. Galhoum (✉) · T. Vincent · E. Guibal (✉) Ecole des mines Alès, Centre des Matériaux des Mines d'Alès, 6 avenue de Clavières, Alès Cedex, France
e-mail: Galhoum_nma@yahoo.com

E. Guibal
e-mail: eric.guibal@mines-ales.fr

A. A. Galhoum · M. G. Mahfouz · N. A. Gomaa Nuclear Materials Authority,
P.O. Box 530, El-Maadi, Cairo, Egypt

S. T. Abdel-Rehem
Chemistry Department, Faculty of Science, Ain Shams University, Cairo, Egypt

A. A. Atia
Chemistry Department, Faculty of Science, Menoufia University, Shebin El-Kom, Egypt

Introduction

High-technology industries are requiring increasing amounts of precious (noble metals, platinum group metals) and strategic metals (such as rare earth metals). More specifically, rare earth elements (comprising lanthanides plus yttrium and scandium) are widely used in electronic devices, metallurgy and the nuclear power industry (Xu and Peng 2009; Zhou et al. 2007). The rarefaction of the resource (for some metals, the horizon of production is limited to a few decades) and monopole for the production of some of these critical metals (which implies geopolitical constraints) is driving research but also political strategies and regulations (Waste Electrical and Electronic Equipment, WEEEs, Directive for European Community, 2002/96/EC, for example) to develop new processes for metal recovery from dilute effluents (uranium leachates, metallurgy effluents) and from secondary resources (coal and phosphate ore residues, etc.) (Sapsford et al. 2012). The circular economy includes the recycling of strategic metals from waste materials: the car industry (plastics and heavy metals), WEEEs (rare earth metals, indium, PGMs, etc.) and municipal solid waste (Innocenzi et al. 2014; Morf et al. 2013).

Metal recovery from solid waste or minerals may consist of pyrometallurgy or hydrometallurgy (chemical leaching or bioleaching) (El-Didamony et al. 2012; Qu and Lian 2013; Yoon et al. 2014; Zhang et al. 2013). The extraction of metals from these leachates or waste streams can be processed by precipitation (Rabatho et al. 2013), solvent extraction (Abreu and Morais 2014; Tunsu et al. 2014; Vander Hoogerstraete and Binnemans 2014; Xie et al. 2014), ion exchange and chelating resins (Abdel-Rahman Adel et al. 2010; Barron et al. 2008; Lokshin et al. 2013; Xiong and Zheng 2010), extractant-impregnated resins (Lee et al. 2010) and biosorption (Das and Das 2013; Hosomomi et al. 2013; Oliveira et al. 2012, 2011; Wu et al. 2011). The selection of the appropriate process depends on the composition of the effluents (i.e., metal concentration, metal speciation, presence of competitor ions) and may face some critical problems: the production of huge amounts of contaminated sludge, difficulty to reach target discharge levels (precipitation) and economic limitations (poor competiveness of solvent extraction at low metal concentration; cost of sophisticated resins). Biosorption is frequently cited as an alternative to conventional ion exchange or chelating resins: the biosorbents may bear similar reactive groups as those present on synthetic resins. Agriculture and fishery residues, subproducts and industrial waste may thus be used for metal binding. Another important challenge in these processes consists of the selectivity of the materials and their capacity to separate target metals from complex effluents.

The group of rare earth elements (REEs) comprises the lanthanide series plus scandium and yttrium. Their most thermodynamically stable form is the trivalent form, M(III). Their physicochemical properties are very close because of their close electronic configurations. The electronic configuration of each lanthanide element is constituted of an inner shell with electrons in the $4f^n$ orbital, shielded by an outer shell composed of electrons in orbitals $5s^2$, $5p^6$, $5d^{1-10}$ and $6s^2$. The slight differences among lanthanide elements are only caused by the electrostatic effect associated with the increase of the shielded nuclear charge through electrons' partial supply of the 4f orbital (which results in lanthanide contraction of the atomic and ionic radius along the lanthanide series). This contraction effect makes possible the separation of REE metals by fractionating methods (Martins and Isolani 2005). However, these differences are so weak that the separation requires numerous steps. Actually, the series of lanthanides can be divided in three families: (1) light REEs, which include La(III), Ce(III), Pr(III), Nd(III) and Sm(III), (2) mild REEs, which include Eu(III), Gd(III), Tb(III) and Dy(III), and (3) heavy REEs, comprised of Ho(III), Er(III), Tm(III), Yb(III), Lu(III) and Y(III) (Cotton 2006; Greenwood and Earnshaw 1997; Sui et al. 2013). The challenge for the REE industry is, in a first step, the separation of REEs from base metals and, in a second step, the separation of individual REEs (Sui et al. 2013). Based on Pearson's theory (hard and soft acid and base theory, HSAB) (Pearson 1966), hard acids (metal ions with high oxidation states, low polarizability and small radii, and the lowest unoccupied molecular orbitals of high energy) react preferentially with hard bases (high electronegativity, highest occupied molecular orbitals of low energy), while, reciprocally, soft acids preferentially react with soft bases. It is possible to use this concept for predicting the reactive groups having an affinity for REEs (Diniz and Volesky 2005a). REE trivalent ions have the behavior

of hard acids, and then they have a higher affinity for hard bases (electron donors with high electronegativity and low polarizability, such as hydroxide, alkoxide, ammonia, carboxylate, carbonate or hydrazine). Hence, chelating agents with O, N and S groups are highly efficient for the selective sorption of lanthanides.

Chitosan has been extensively studied for metal biosorption (Guibal 2004), benefiting from the presence of hydroxyl and amino groups. Chitosan is a heteropolymer comprised of D-glucosamine units and acetyl-D-glucosamine units linked by β(1 → 4) bonds. The amine groups on chitosan are responsible for metal binding through different mechanisms, including (1) metal cation chelation on free amino groups (via the free electron doublet of nitrogen) at near neutral pH and (2) electrostatic attraction/ion exchange of metal anions on protonated amino groups (in acidic solutions). However, the affinity of the sorbent strongly depends on the intrinsic properties of metal cations (HASB theory): for example, in the case of REEs pristine chitosan has limited sorption capacities, and it is generally necessary to graft new functional groups and/or increase their density at the surface of the sorbent to reach appreciable sorption capacities. Several chelating ligands such as catechol, iminodiacetic acid, iminodimethylphosphonic acid, EDTA and DETPA (and similar functional groups, Elwakeel et al. 2009), phenylarsonic acid or serine (Elwakeel and Atia 2014; Elwakeel et al. 2014; Hakim et al. 2007; Oshita et al. 2009; Ren et al. 2013; Repo et al. 2013; Roosen and Binnemans 2014), and amino acid moieties (glycine, valine, leucine and serine) (Oshita et al. 2007) were used to functionalize crosslinked chitosan for the sorption of uranium, PGMs, REEs and associated metal ions. Grafting supplementary amino groups onto the chitosan backbone may contribute not only to an increase in the density of sorption sites, but also to the enhancement of sorbent affinity by appropriate steric distribution of reactive groups (Wang et al. 2011): increasing the number of chelate rings increases the stability of complex formed by polyamine. Hence, diethylenetriamine (DETA) exhibits different kinds of coordination modes for interacting with metal ions: for example, five-membered chelating rings increase the metal sorption capacity (Xu et al. 2013). Zhao et al. reported the modification of chitosan with EDTA, DTPA and EGTA [ethylene glycol-bis(2-aminoethylether)-N,N,N′,N′-tetraacetic acid] for the manufacturing of magnetic and nonmagnetic sorbents for the recovery of heavy metals (Zhao et al. 2013, 2015). They pointed out the double effect of EDTA, DTPA and EGTA, which contribute to both the crosslinking of chitosan and the chelation of metal ions.

Chitosan can be considered a very interesting base material for the development of chelating and ion-exchange resins, benefiting from the easy functionalization of hydroxyl groups and amino groups and of the hydrophilic behavior associated with the presence of numerous hydroxyl groups (more hydrophilic than conventional synthetic materials, such as polystyrene-divinylbenzene, polyethylene and polyurethane) (Gao et al. 2002). However, the solubility of chitosan in acid media (with the remarkable exception of sulfuric acid solutions) is a serious drawback that can be overcome by crosslinking for improving chemical and/or mechanical properties (Jayakumar et al. 2005). Depending on the crosslinking method, the sorption affinity for the target metal may be strongly affected (and sometimes completely inhibited) because of the modification of the availability and reactivity of functional groups and the modification of crosslinked chitosan with chelating moieties (Oshita et al. 2009). Therefore, novel chitosan resins possessing chelating moieties have been developed by using a crosslinked chitosan resin as a base material. A huge number of chitosan derivatives have been used for the sorption of metal ions by grafting new functional groups onto the chitosan backbone. Another important drawback of chitosan-based materials is associated with the poor porosity properties of chitosan (microporosity, reduced specific surface area, etc.). This means that material must be modified to improve the uptake kinetics by physical modification (designing hydrogels, foams, etc.) (Allouche et al. 2014; Ruiz et al. 2002a, b) or playing with the size of sorbent particles. Decreasing the size of particles contributes to increasing the surface area and decreasing the resistance to intraparticle diffusion (at the macroscale). However, reducing the size of sorbent particles (to the submicron size) leads to difficulties in recovering spent materials by conventional settling, filtration or centrifugation processes at the end of the sorption process. To minimize this drawback, a solution may be to design magnetic nano-based particles by coating them with chitosan (which can be further functionalized by grafting new reactive groups) (Xue et al. 2013; Zhou et al. 2010). An external magnetic field allows separating spent sorbent particles at the end of the sorption process.

Previous studies have reported the synthesis and characterization of a hybrid material made of DETA-functionalized chitosan deposited on magnetic nano-based particles (Fe_3O_4) and their application to uranium recovery (Mahfouz et al. 2015). This material was used in the present study for the recovery of three REEs belonging to light [Nd(III)), mild (Dy(III)] and heavy [Yb(III)] REE families in batch tests. The sorption experiments evaluated the influence of pH, investigated sorption isotherms and uptake kinetics, and calculated the thermodynamic parameters. Finally, REE desorption from loaded sorbent was also investigated with the objective of recycling the sorbent.

Experimental

Reagents and analysis

Chitosan (90.5 % deacetylation degree) was supplied by Sigma-Aldrich (France). Diethylenetriamine (98 %) was obtained from Sigma-Aldrich; epichlorohydrin (>98 %), 1,4-dioxane (99.9 %) and ethanol were purchased from Fluka Chemika (Switzerland). Sodium hydroxide solution (30 %) was supplied by Chem-Lab. NV and all other chemicals were Prolabo products and were used as received.

$NdCl_3$, $DyCl_3{\cdot}xH_2O$ and $YbCl_3{\cdot}6H_2O$ salts were purchased from Sigma-Aldrich. The salts were burned off at 900 °C for 3 h. Stock solutions of the rare earth ions Nd(III), Dy(III) and Yb(III) were prepared by mineralization of the corresponding salts in concentrated sulfuric acid under heating before being diluted with demineralized water to a final concentration of 1000 mg l^{-1}. The working solutions were prepared by appropriate dilution of the stock solutions immediately prior to use. The metal concentrations in both initial and withdrawn samples were determined by an inductively coupled plasma atomic emission spectrometer (ICP-AES JY Activa M, Jobin-Yvon, Longjumeau, France).

Preparation of sorbent

Hybrid magnetic chitosan magnetic nano-based particles were prepared by chemical coprecipitation of Fe(II) and Fe(III) ions by NaOH in the presence of chitosan followed by hydrothermal treatment (Mahfouz et al. 2015; Namdeo and Bajpai 2008). Chitosan was reacted with a 1:2 molar ratio solution of iron(II) sulfate and iron(III) chloride before being precipitatated at pH 10.2 with NaOH at 40 °C and then at 90 °C under reflux. A crosslinking treatment was operated using an alkaline epichlorohydrin solution at 40–50 °C (Wan Ngah et al. 2002). The grafting of DETA was performed in two steps: (1) grafting of spacer arms and (2) immobilization of DETA (Oshita et al. 2007). The materials were systematically rinsed with demineralized water after each step, and the sorbent was finally freeze-dried for 214 h.

Sorption experiments

Batch experiments were carried out by contact of 20 mg functionalized chitosan sorbent (m, g) with 100 ml aqueous metal ion solution (V, l) of 100 mg l^{-1} (C_0, mg metal l^{-1}) in a polypropylene centrifuge tube. The suspension was agitated on a reciprocal shaker (agitation speed: 300 rpm) for 4 h. After phase separation, the residual concentration (C_{eq}, mg metal l^{-1}) was determined by ICP-AES, and the sorption capacity (q_{eq}, mg metal g^{-1}) was determined by the mass balance equation:

$$q_{eq} = (C_0 - C_{eq})V/m \quad (1)$$

The effect of pH was analyzed by the same experimental procedure: the value of the initial pH was varied between 1 and 7; the pH was not controlled during the sorption but was monitored at the end of the experiment. For the study of sorption isotherms, the initial pH was set to 5, and the concentration of the metal was varied between 0 and 300 mg metal l^{-1}. The temperature was systematically set to 27 ± 1 °C, except for the specific study of temperature effect (thermodynamic study) where three temperatures were used (i.e., 17 °C, 27 and 37 °C). Uptake kinetics were obtained by withdrawing samples at a given contact time (magnetic separation) and analysis of the residual concentration in a function of time over 4 h. The study of sorption/desorption performance followed basically the same procedure: a given amount of sorbent was mixed for 4 h with a 100 mg metal l^{-1} solution at pH 5; after being magnetically separated and rinsed, the sorbent was mixed with 100 ml of thiourea aqueous solution (0.5 M, slightly acidified with sulfuric acid) for 1 h. After magnetic separation and rinsing, the sorbent was recycled (using the same procedure).

Results and discussion

Preparation and physicochemical characteristics of the sorbent

The synthesis and characterization of the sorbent were already described (Mahfouz et al. 2015). Detailed information is available in the Additional Material Section. The purpose of this section is only to report the main conclusions on the properties of this material obtained from (1) the one-pot synthesis of chitosan-coated magnetic nanoparticles and (2) DETA-grafted magnetic composite (see the Additional Material Section, Figure AM1) (Mahfouz et al. 2015).

The weight loss of the sorbent was determined at different temperatures to evaluate the residual water content (about 4 % at 110 °C) and the fraction of magnetite in the final product (about 47 % at 600 °C).

Elemental analysis showed an increase in nitrogen content in the hybrid material after DETA grafting from 1.7 to 4.8 % (Mahfouz et al. 2015) (i.e., 1.21 and 3.43 mmol N g^{-1} sorbent). This significant change proves the efficiency of the immobilization of the polyamine compound at the surface of the chitosan-magnetite composite. Based on the magnetite content in the final sorbent (i.e., 49 %), the mole amounts of nitrogen in the organic compartment of the sorbent are 2.38 and 6.72 mmol N g^{-1}, respectively. The increase in nitrogen content (about 2.82 times) is quite close to the stoichiometric increase in the nitrogen content based on the proposed structure (Figure AM1, See Additional Material Section). This means that more than 90 % of nitrogen on crosslinked chitosan has been substituted with DETA. This is also confirmed by the FTIR analysis where the intensity of the characteristic bands of amino groups substantially increased (identified at 1387 cm^{-1}), while the presence of a band at 568 cm^{-1} was assigned to the presence of magnetite (Fe_3O_4) (i.e., Fe–O, stretching vibration) (see the Additional Material Section, Figure AM2) (Mahfouz et al. 2015).

The presence of magnetite was confirmed by the analysis of XRD patterns (see the Additional Material Section, Figure AM3): the peaks were observed at $2\theta = 30°, 35°, 43°, 53°, 57°$ and 63° for indices (220), (311), (400), (422), (511) and (440), respectively. These peaks are characteristic of Fe_3O_4 magnetite nanoparticles with a spinel structure and high magnetic properties. However, some additional small peaks at $2\theta = 21°, 33°$ and 41° may be indicative of the presence of some impurities in the form of α- or γ-Fe_2O_3 (i.e., maghemite) (Russo et al. 2012). The Debye-Scherrer equation was used [on index (311), the highest and largest peak] for calculating the crystal sizes: this was about 6.5 nm. The TEM photographs showed a kind of aggregation phenomenon to form agglomerates of sizes ranging between 10 and 30 nm (see the Additional Material Section, Figure AM4) (Mahfouz et al. 2015). This agglomeration is associated with a magnetic dipole-dipole attraction mechanism reinforced by the small particle sizes. These nano-based particles remained small in size, suggesting limited resistance to intraparticle diffusion.

The magnetic properties were tested with a vibrating sample magnetometer, and the saturation magnetization was found close to 20 emu g^{-1} with no remanence or coercivity (see Additional Material Section, Figure AM5): this means that the materials have the properties of superparamagnetic particles. These materials will be readily collected when applying an external magnetic field (Mahfouz et al. 2015).

Sorption properties

Sorption as a function of the pH

The pH is a critical parameter in the sorption of metal ions on ion exchange and chelating resins because it may affect the chemistry of metal ions (changing metal speciation) and the surface properties of the resin (acid-base properties, charge of functional groups), which, in turn, influence the affinity of the resin for target metal ions. Figure 1 reports the progressive increase of the sorption capacity with increasing pH: the curves for Nd(III), Dy(III) and Yb(III) overlap (in molar units). Changing the pH will not contribute to improving the selective separation among these metals representing the three REE families. The sorption increases with pH up to 5 and tends to stabilize above this equilibrium value. When the pH increases, the protonation of the amino groups decreases: their capacity to chelate/complex REE cations is enhanced. Actually, a great dispersion of values appears around equilibrium pH 6. Figure AM1 (in Additional Material Section) reports pH variation with metal sorption. Within a pH range of 1–3, the equilibrium pH remains close to the initial pH value, while in the range of initial pH 3–5, the equilibrium pH

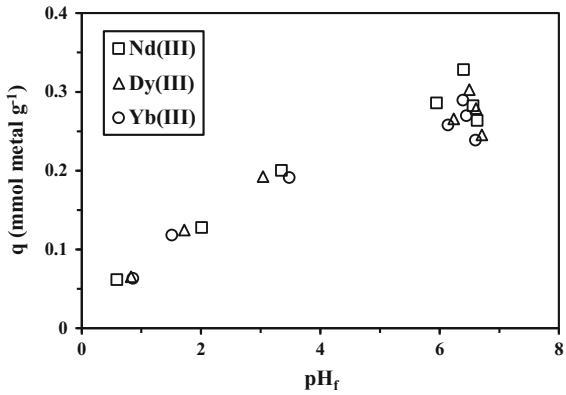

Fig. 1 Effect of pH on Nd(III), Dy(III) and Yb(III) sorption using DETA-functionalized chitosan magnetic nano-based particles. (C_0: 100 mg metal l^{-1}; $T = 27$ °C; contact time: 4 h; sorbent dosage, SD 0.2 g l^{-1})

tends to increase by 1 or 2 pH units. At pH 6, the equilibrium pH tends to stabilize. This may be attributed to the buffering effect of amine functions (especially from chitosan support): with a pK_a close to 6.3–6.7, amine groups of chitosan (and probably from DETA) bind protons (leading to pH increase). A slight decrease in sorption is observed for initial pH 6 (and higher) (and equilibrium pH close to 6.3). This is probably due to a change in metal speciation: metal ions begin to form hydrolyzed products with a probable loss of affinity for amino groups. These phenomena of hydrolysis (at high pH values associated with precipitation) and the weak stability of magnetite particles in acidic solutions (dissolving of Fe_3O_4, especially at pH lower than 1.5–2) allow concluding that the sorbent should be preferentially operated in the pH range 2–5. For further experiments, the pH was initially set at pH 5 (not controlled during sorption but monitored at the end of the experiment). Maximum sorption capacities are obtained for the three REEs at initial pH 5 with sorption capacities close to 47–50 mg metal g^{-1} (i.e., in the range 0.29–0.33 mmol metal g^{-1}). In these preliminary results, the DETA-functionalized chitosan magnetic nano-based particles can be ranked according to Nd(III) > Dy(III) > Yb(III) in molar units, although the differences are not very marked.

The protonation of amino groups may explain the decrease in sorption performance. However, the impact of the dissociation of sulfuric acid (which is used for pH control) can also influence the sorption properties. Indeed, the presence of HSO_4^- (in weakly acidic solutions) may involve competition effects: the formation of complexes with lower affinity for amine groups influences the sorption efficiency (Elyamani and Shabana 1985). Based on the sorbent stability, precipitation issues (above pH 6–6.5), pH variation and sorption increase with pH, further experiments were performed at initial pH 5.

The sorption of Eu(III) with chitosan has been reported to involve contributions of amine and hydroxyl groups from parallel chains of the biopolymer (Cadogan et al. 2014). By analogy, it is possible to suggest that trivalent cations interact with either chitosan amino groups or amino groups held on the DETA substitutes with the contribution of hydroxyl groups of the chitosan backbone. Multidentate N-donors interact with lanthanides by the formation of complexes with 6, 7, 8 and 9 (and more) donor atoms (Greenwood and Earnshaw 1997). The presence of vicinal nitrogen groups (held by neighbor chitosan chains and DETA substitutes) is thus important for enhancing REE sorption.

Effect of contact time and kinetic studies

Figure 2 shows the kinetic profiles for Nd(III), Dy(III) and Yb(III) sorption using the DETA-functionalized chitosan magnetic nano-based particles. The sorption capacity increases with time in two steps: (1) a first very steep initial section that represents about 80 % of total sorption occurs within the first 10 min of contact; (2) a second slow phase lasts for 3–4 h to reach

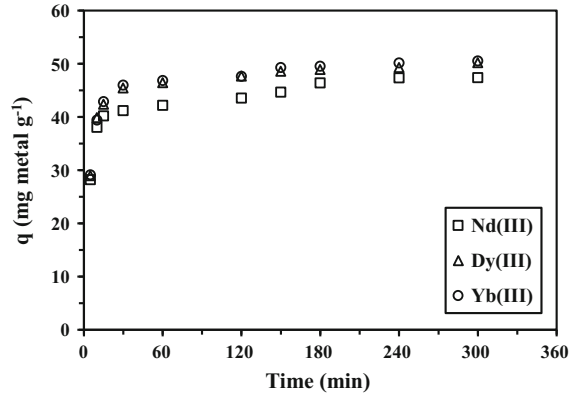

Fig. 2 Uptake kinetics for the sorption of Nd(III), Dy(III) and Yb(III) using DETA-functionalized chitosan magnetic nano-based particles (C_0: 100 mg metal l^{-1}; pH: 5; $T = 27$ °C; sorbent dosage, SD 0.2 g l^{-1})

Table 1 Modeling of uptake kinetics using the PFORE and PSORE models for Nd(III), Dy(III) and Yb(III) sorption (at 27 °C and pH_i 5)

Metal ion	$q_{max,exp.}$ (mg g^{-1})	PFORE			PSORE		
		k_1 (min^{-1})	q_{eq} (mg g^{-1})	R^2	$k_2 \times 10^3$ (mg g^{-1} min^{-1})	q_{eq} (mg g^{-1})	R^2
Nd(III)	47.4	0.012	11.7	0.851	3.39	48.3	0.999
Dy(III)	50.4	0.0198	11.4	0.932	4.34	50.8	0.999
Yb(III)	50.7	0.0150	11.7	0.882	2.76	50.5	0.986

equilibrium. About 90 % of the total sorption occurs within the first 30 min of contact. Sorption kinetics are generally controlled by a series of coupled mechanisms including the proper reaction rate but also diffusion mechanisms. The bulk diffusion (diffusion in the solution) is generally not limiting, providing the solution is perfectly agitated. The external diffusion (or diffusion in the film surrounding the particle) is mainly active in the first minutes of contact, while the intraparticle diffusion is especially active for poorly porous materials (depending on the sorbent particle size, pore size, etc.). Chitosan is generally a poorly porous material with a low specific surface area (a few m^2 g^{-1}). The sorption kinetics usually require several hours (24–48 h, depending on the experimental conditions) to reach equilibrium. Decreasing the size of sorbent particles or elaborating alternate conditionings (gel beads) is necessary for achieving fast kinetics (Ruiz et al. 2002a, b). Elaborating nano-based particles, which consist of nanoparticles of magnetite coated with chitosan, allows reducing the diffusion thickness and decreasing the resistance to intraparticle diffusion. The two-step profile of uptake kinetics can thus be interpreted as the successive phases of (1) surface sorption associated with the resistance to film diffusion (within the first 10 min of contact), followed by (2) the swelling of the DETA-functionalized chitosan coating and the contribution of the resistance to intraparticle diffusion (which is, however, limited by the small size of sorbent particles).

Different models have been tested for fitting the experimental uptake kinetics; the pseudo-first order rate equation (PFORE), pseudo-second order rate equation (PSORE) and simplified resistance to the intraparticle diffusion equation (sRIDE) were employed to examine the kinetics data (Qiu et al. 2009). The linear forms of PFORE and PSORE are reported in Eqs. (2) and (3), respectively:

$$\log\left(q_e - q(t)\right) = \log q_e - \frac{k_1}{2.303}t \tag{2}$$

$$\frac{t}{q(t)} = \frac{1}{k_2 q_e^2} + \frac{1}{q_e}t \tag{3}$$

where q_e and $q(t)$ (mg g^{-1}) are the sorption capacities at equilibrium and time t (min), respectively. k_1 (min^{-1}) and k_2 (g mg^{-1} min^{-1}) are the rate constant of PFORE and PSORE, respectively.

The simplified model of resistance to intraparticle diffusion (sRIDE, the so-called Weber and Morris equation) is reported in Eq. (4):

$$q(t) = k_{int.}t^{0.5} + c \tag{4}$$

where $k_{int.}$ (mg g^{-1} $min^{-0.5}$) is the intraparticle diffusion constant.

Table 1 reports the parameters of the PFORE and PSORE models: the analysis of the correlation coefficients (which is confirmed by the regression plots of experimental data; see the Additional Material Section, Figure AM7) shows that the PSORE model fits the experimental data much better than the PFORE model. Figure AM7 and Table AM1 (Additional Material Section) show that the simplified RIDE model (Weber and Morris equation) does not fit the experimental data. Two sections can be identified corresponding to the two phases of the process.

The PSORE model is frequently associated with the chemical sorption mechanism (involving valence forces such as the sharing or exchange of electrons, complexation, coordination and chelation) (Hu et al. 2011). The general sorption process can thus be described as the combination of the physical and fast sorption of metal ions for the first minutes of contact followed by the slow uptake mechanisms involving chemical bonding and contribution of the swelling effect and resistance to intraparticle diffusion.

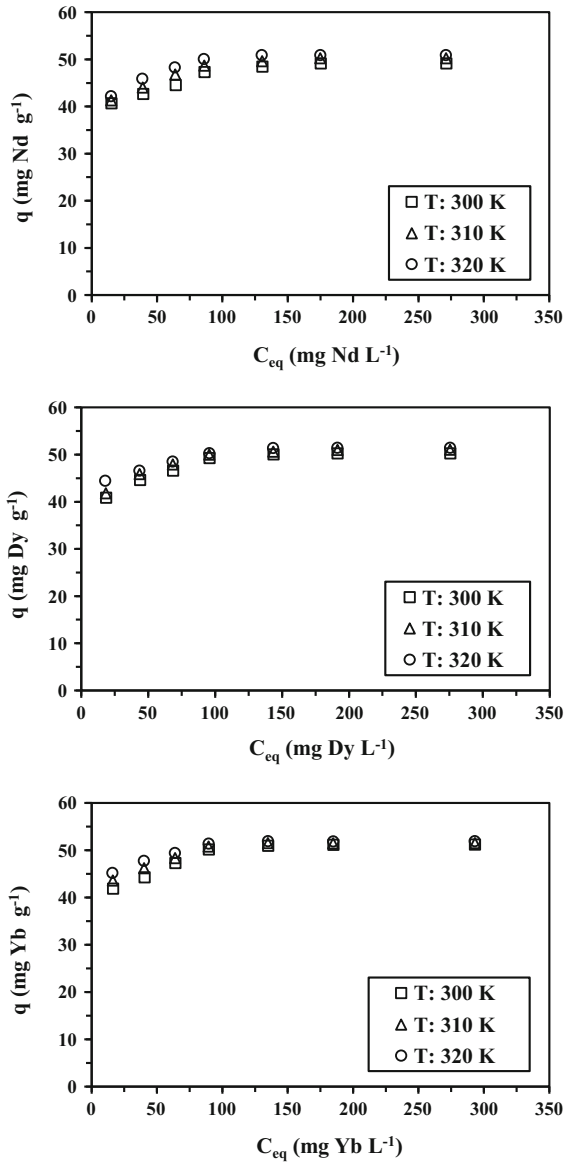

Fig. 3 Sorption isotherms of Nd(III), Dy(III) and Yb(III) sorption isotherms using DETA-functionalized chitosan magnetic nano-based particles at different temperatures (C_0: 100 mg metal l^{-1}; pH: 5; $T = 27$ °C; contact time: 4 h; sorbent dosage, SD 0.2 g l^{-1})

Sorption isotherms and thermodynamics

The sorption isotherms [$q_{eq} = f(C_{eq})$] represent the distribution of the solute (at different initial concentrations, C_0, but at the same temperature and pH) between the liquid phase (C_{eq}) and solid phase (q_{eq}). Figure 3 shows the sorption isotherms for Nd(III), Dy(III) and Yb(III) using DETA-functionalized chitosan magnetic nano-based particles at initial pH 5 and at three different temperatures, 27, 37 and 47 °C (300, 310 and 320 K). The superimposition of the curves at the three different temperatures shows that the temperature has a limited effect on the sorption properties. The curves are represented by a sharp initial increase in sorption capacity: for a residual concentration of 10–15 mg metal l^{-1}, the sorption capacity reaches 40 mg metal g^{-1}; this means about 80 % of the maximum sorption capacity. The sorption capacity progressively increases up to a maximum sorption capacity close to 50–52 mg metal g^{-1}, regardless of the type of sorbent and the temperature. The asymptotic plateau is consistent with a phenomenon of monolayer saturation. Sorption isotherms can be modeled using different equations (Foo and Hameed 2010): Langmuir (Langmuir 1918), Freundlich (Freundlich 1906), Temkin (Temkin 1940) and Dubinin–Radushkevich (Dubinin et al. 1947), for example.

The Langmuir model is based on the assumption that sorption sites are identical and energetically equivalent, and that sorption occurs as a monolayer coverage (Foo and Hameed 2010; Langmuir 1918). It can be represented, in its linearized form, by Eq. (5):

$$\frac{C_{eq}}{q_{eq}} = \frac{C_{eq}}{q_{max}} + \frac{1}{bq_{max}} \tag{5}$$

where q_{max} is the maximum sorption capacity of the sorbent (mg metal g^{-1}), and b is the Langmuir sorption constant (L mg^{-1}), respectively.

The Freundlich isotherm model is based on the assumption of a heterogeneous distribution of the sorption sites (basically corresponding to heterogeneous material in terms of reactive groups) (Foo and Hameed 2010; Freundlich 1906). The Freundlich equation (linearized form) is represented by Eq. (6):

$$\ln q_e = \ln K_f - \frac{1}{n} \ln Ce \tag{6}$$

where K_f is the Freundlich isotherm constant, and n (dimensionless) is the heterogeneity factor.

The Dubinin–Radushkevich (D–R) model is usually employed for discriminating the nature of sorption processes as a physical or chemical mechanism. The D-R equation is given by Eq. (7) (Dubinin et al. 1947; Foo and Hameed 2010).

Table 2 Modeling of sorption isotherms using the Langmuir and Freundlich equations for Nd(III), Dy(III) and Yb(III) sorption (at different temperatures)

Metal ion	T (K)	$q_{max,exp.}$ (mg metal g^{-1})	Langmuir model			Freundlich model		
			$q_{max,calc.}$ (mg metal g^{-1})	b (L mg^{-1})	R^2	1/n	K_F	R^2
Nd(III)	300	49.2	50.8	0.132	0.999	11.6	31.0	0.934
	310	50.3	51.8	0.151	0.999	11.6	32.0	0.924
	320	50.9	52.1	0.197	0.999	12.7	33.8	0.878
Dy(III)	300	50.3	51.2	0.091	0.996	12.2	32.8	0.923
	310	51.0	52.1	0.201	0.999	13.1	34.3	0.914
	320	51.5	52.4	0.240	0.999	16.8	37.6	0.938
Yb(III)	300	51.2	52.4	0.191	0.999	12.6	33.8	0.903
	310	51.5	52.4	0.255	0.999	15.6	36.8	0.900
	320	51.9	52.6	0.331	0.999	19.1	39.6	0.894

Table 3 Modeling of sorption isotherms using the Dubinin–Radushkevich and the Temkin equations for Nd(III), Dy(III) and Yb(III) sorption (at different temperatures)

Metal ion	T (K)	D-R isotherm				Temkin isotherm		
		q_s (mg metal g^{-1})	$K_{ad} \times 10^5$ (mol^2 kJ^{-2})	E_{DR} (kJ mol^{-1})	R^2	A_T (L mg^{-1})	B_T (J mol^{-1})	R^2
Nd(III)	300	48.9	5.83	0.112	0.924	7.26	3.90	0.935
	310	50.2	5.00	0.129	0.982	7.43	3.96	0.930
	320	51.1	3.77	0.129	0.978	8.55	3.70	0.885
Dy(III)	300	50.4	4.11	0.112	0.941	8.15	3.75	0.929
	310	51.0	3.32	0.129	0.961	9.08	3.56	0.928
	320	51.5	2.93	0.129	0.952	12.69	2.87	0.939
Yb(III)	300	51.4	4.25	0.112	0.970	8.57	3.70	0.905
	310	51.7	2.96	0.129	0.947	11.53	3.07	0.902
	320	52.0	2.10	0.158	0.943	15.12	2.55	0.896

$$\ln\ q_e = \ln q_D - K\varepsilon^2 \quad (7)$$

where q_D is the theoretical saturation capacity, and ε is the Polanyi potential [given by $\varepsilon = RT\ \ln(1 + 1/C_{eq})$]. K is related to the mean free sorption energy per molecule of sorbate, E_{DR} (kJ mol^{-1}). E_{DR} provides information about the chemical and physical sorption (the discriminating value being physical < 8 kJ $mol^{-1} <$ chemical sorption) and can be determined according to Eq. (8):

$$E_{DR} = (2K)^{-1/2} \quad (8)$$

Tables 2 (for the Langmuir and Freundlich models) and 3 (for the Temkin and Dubinin–Radushkevich models) show the parameters of the models and the quality of their fit (through the comparison of their correlation coefficients). In addition, Figures AM8 and AM9 (see Additional material Section) show the linear plots of the Langmuir and D-R fits of experimental data. Table 2 confirms that the Langmuir equation fits the experimental data better than the Freundlich equation: this is consistent with the asymptotic trend of the isotherm (compared to the exponential form of the Freundlich equation). Table 3 shows that both q_{max} and b slightly increase with temperature: the sorption is thus expected to be slightly endothermic. The "favorability" of the sorption can be evaluated using the coefficient R_L (dimensionless) (Foo and Hameed 2010), which is calculated by Eq. (9):

$$R_L = \frac{1}{1 + bC_0} \tag{9}$$

where C_0 is the initial concentration of the metal ion in the relevant experiment. The calculated values of the dimensionless factor R_L for DETA-functionalized chitosan magnetic nano-based particles lie between 0.02 and 0.26 for Nd(III), between 0.01 and 0.29 for Dy(III) and between 0.01 and 0.17 for Yb(III), regardless of the concentration and temperature range. All R_L values being smaller than 1.0, the sorption of Nd(III), Dy(III) and Yb(III) ions on the designed sorbent is very favorable. The Langmuir model assumes that the sorption process occurs as a monolayer on a surface with a finite number of identical sites, which are homogeneously distributed over the sorbent surface. Although the fact that the equation mathematically fits the experimental data does not necessarily means that that the hypotheses of the model are verified, this is a first indication of possible characteristics of the phenomenon (which must be verified by physical observations). The composition of the chemically modified surface of the sorbent is heterogeneous because of the presence of free amino groups of chitosan and DETA, which may have different affinities for metal ions. Despite these differences, the sorption isotherm does not show heterogeneities.

Table 2 also reports the values of the parameters of the Freundlich model: the correlation coefficients are lower than those found with the Langmuir equation. When the heterogeneity factor (i.e., n) is higher than 1, the sorption is favorable in the whole range of concentrations, while when n is below 1, the sorption is only favorable at high solute concentrations (Foo and Hameed 2010). In the present case, the heterogeneity factor was systematically below 0.1: the sorption is only favorable at a high residual metal concentration.

In the case of the Dubinin–Radushkevich (D–R) isotherm, the plot of ln q_{eq} versus ε^2 gives a straight line with a slope K and an intercept ln q_D as shown in Figure AM9 (see Additional Material Section). Table 3 reports the values of the parameters of the D-R equation for the different systems. The mean sorption energy (E_{DR}) represents the free energy necessary for transferring 1 mole of solute from infinity (in solution) to the surface of the sorbent. The mean sorption energies (E_{DR}) for the sorption of Nd(III), Dy(III) and Yb(III) ions on DETA-functionalized chitosan magnetic nano-based particles are systematically below 8 kJ mol^{-1}: metal binding essentially proceeds by physical sorption (consistent with conclusions proposed for uptake kinetics). In addition, the positive values of E_{DR} indicate that the sorption process is endothermic: a higher temperature slightly enhances sorption.

The Temkin model assumes that the free energy of sorption is a function of the surface coverage (Foo and Hameed 2010; Temkin 1940). The isotherm is described by Eq. (10):

$$q_q = B_T \ln C_{eq} + B_T \ln A_T \tag{10a}$$

$$B_T = RT/b_T \tag{10b}$$

where A_T is the equilibrium binding constant corresponding to the maximum binding energy, B_T is a constant related to the surface heterogeneity of the sorbent, R is the universal gas constant (8.314 J K^{-1} mol^{-1}), b_T is a constant related to adsorption heat, T is the temperature (K), and R is the ideal gas constant (8.314 J mol^{-1} K^{-1}). The constants of the model can be obtained from the slope and intercept of the linear plot of q_{eq} versus ln C_{eq}. Table 3 summarizes the values of these parameters. The constant A_T reflects the initial sorption heat for the sorbent: the greater the A_T value is, the higher the sorption heat, and the greater the affinity of the sorbent for the sorbate. The A_T values for Yb(III) were higher than the values of Dy(III) and Nd(III) ions: Yb(III) ions are more likely to be bound on the sorbent than Dy(III) and Nd(III) ions. Furthermore, the affinity of the surface-reactive groups for metal ions increases with temperature. The order of affinity follows the trend: Yb(III) > Dy(III) > Nd(III); however, this should be considered as indicative, since the Temkin model fits the experimental data less accurately than the Langmuir equation.

Figure 4 shows the effect of increasing temperature on Nd(III), Dy(III) and Yb(III) sorption using DETA-functionalized chitosan magnetic nano-based particles. The maximum sorption capacity slightly increases with temperature. The thermodynamic parameters [i.e., Gibbs free energy change, $\Delta G°$ (kJ mol^{-1}), enthalpy change, $\Delta H°$ (kJ mol^{-1}) and entropy change, $\Delta S°$ (J mol^{-1} K^{-1})] can be obtained from the van't Hoff equation, Eqs. (11) and (12):

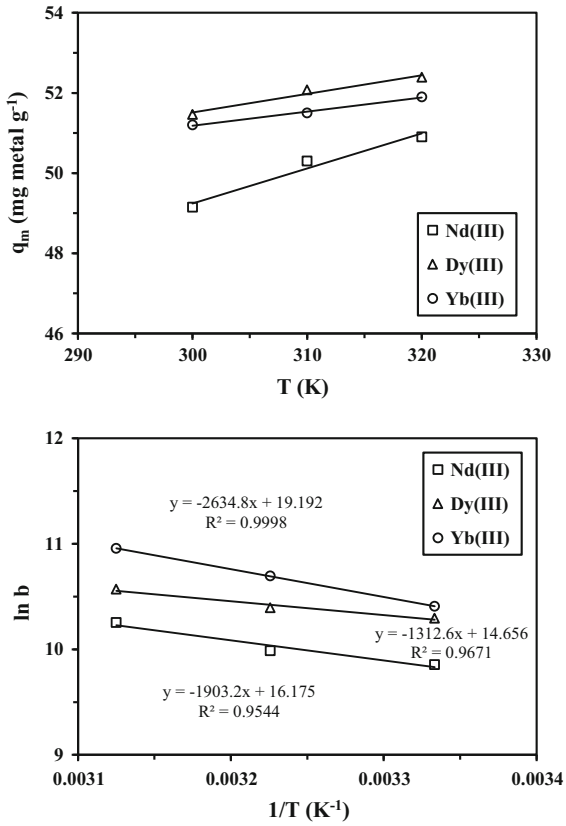

Fig. 4 Thermodynamic properties of Nd(III), Dy(III) and Yb(III) sorption using DETA-functionalized chitosan magnetic nano-based particles: variation of q_{max} with temperature and van't Hoff plots of ln b against 1/T (pH: 5; $T = 300$, 310 and 320 K; contact time: 4 h; sorbent dosage, SD 0.2 g l^{-1})

$$\ln b = \frac{-\Delta H^{\circ}}{RT} + \frac{\Delta S^{\circ}}{R} \quad (11)$$

$$\Delta G^{\circ} = \Delta H^{\circ} - T\Delta S^{\circ} \quad (12)$$

where T is the absolute temperature (Kelvin). The values of enthalpy change (ΔH°) and entropy change (ΔS°) were obtained by the slope and the intercept of the plot of ln b versus 1/T (Fig. 4); the constants are reported in Table 4. The positive values of enthalpy change (ΔH°) and the decrease in Gibbs free energy change with the increase of the temperature confirm that the sorption mechanism is endothermic: the reaction is slightly enhanced at higher temperature. On the other hand, the positive values of the entropy change (ΔS°) mean that the "disorder" of the system increases after metal sorption. This increase in the entropy is probably associated with the water release during metal sorption of rare earth metal ions (which are initially hydrated in solution). The fact that systematically $|\Delta H^{\circ}|$ is lower than $|T\Delta S^{\circ}|$ means that the sorption process is controlled by entropic rather than enthalpic changes (Rahmati et al. 2012). Marcus (1997) reports the thermodynamic parameter of hydrated ions. The entropy changes of sorption (like other thermodynamic data) do not follow a clear trend regarding the classification of REEs (light, mild and heavy), and it is not possible to correlate these values to the thermodynamic values of hydrated species. The lower dispersion of data was obtained comparing entropy changes of sorption with the enthalpy of formation of hydrated species ($\Delta H^{f}_{\text{hydr.}}$, kJ mol^{-1}), which varies according to the sequence: Dy(III) (−699)–Nd(III) (−696)–Yb(III) (−675).

Comparison of sorption properties with other sorbents

The sorption of different materials for Nd(III), Dy(III) and Yb(III) is compared to the sorption capacities obtained with DETA-functionalized chitosan magnetic nano-based particles (Table 5). Different experimental conditions make the comparison of sorption performance complex. However, the table shows that the sorbent has comparable sorption properties for the binding of selected REEs in slightly acidic to neutral solutions. Some materials have significantly higher sorption properties, such as activated charcoal for Dy(III) (Qadeer and Hanif 1995), phosphorous functionalized sorbent for Nd(III) (Park and Tavlarides 2010), and iminodiacetic resin (Xiong et al. 2006) or *Sargassum* biomass (Diniz and Volesky 2005a) for Yb(III). However, in most cases the DETA-functionalized chitosan magnetic nano-based particles have comparable sorption properties for selected REEs. The main advantage of the present sorbent is the fast kinetics of sorption associated with its nano-/micrometric size and the easy recovery of spent material at the end of the sorption process through magnetic attraction.

Metal desorption and sorbent recycling

Metal desorption and sorbent recycling are important issues for the competitiveness of sorbent materials. Frequently, the eluent selected for metal release is

Table 4 Thermodynamic parameters for Nd(III), Dy(III) and Yb(III) sorption

Metal ion	$\Delta H°$ (kJ mol^{-1})	$\Delta S°$ (J mol^{-1} K^{-1})	T (K)	$\Delta G°$ (kJ mol^{-1})	$T\Delta S°$ (kJ mol^{-1})	R^2
Nd(III)	15.8	134	300	−24.5	40.3	0.954
			310	−25.9	41.7	
			320	−27.2	43.0	
Dy(III)	10.9	122	300	−25.6	36.6	0.967
			310	−26.9	37.8	
			320	−28.1	39.0	
Yb(III)	21.9	160	300	−26.0	47.9	0.999
			310	−27.6	49.5	
			320	−29.2	51.1	

Table 5 Comparison of Nd(III), Dy(III) and Yb(III) sorption performance for different sorbents

Sorbent	Metal	pH range	q_m (mg metal g^{-1})	Reference
EDTA and DTPA functionalized chitosan	Nd(III)	3–6	55	Roosen and Binnemans (2014)
Phosphonic acid functionalized silica microspheres	Nd(III)	2.8	45	Melnyk et al. (2012a)
Ion imprinted polymer particles	Nd(III)	7.5	33	Krishna et al. (2005)
Phosphorus functionalized adsorbent	Nd(III)	6	160	Park and Tavlarides (2010)
Yeast cells	Nd(III)	1.5	10–12	Vlachou et al. (2009)
Mordenite containing tuff	Nd(III)	5.5–6.5	13	Kozhevnikova and Tsybikova (2008)
DETA-functionalized chitosan magnetic nano-based particles	Nd(III)	5	49–51	This work
Oxidized multi-walled carbon nanotubes	Dy(III)	4–6	78	Koochaki-Mohammadpour et al. (2014)
11-Molybdo-vanadophosphoric acid supported on Zr modified mesoporous silica SBA-15	Dy(III)	4–5	42–53	(Aghayan et al. 2013)
Activated charcoal	Dy(III)	4	294	Qadeer and Hanif (1995)
Phosphonic acid-functionalized porous microspheres	Dy(III)	4.8	32–49	Melnyk et al. (2012b)
DETA-functionalized chitosan magnetic nano-based particles	Dy(III)	5	51–52	This work
Sargassum	Yb(III)	5	160	Diniz and Volesky (2005a)
Turbinaria conoides	Yb(III)	4.9	34	Vijayaraghavan et al. (2011)
Pseudomonas aeruginosa	Yb(III)	6–7	56	Texier et al. (1999)
Imino-diacetic acid resin	Yb(III)	5.1	187	Xiong et al. (2006)
DETA-functionalized chitosan magnetic nano-based particles	Yb(III)	5	51–52	This work

based on the effect of pH on sorption: acidic pH is used for desorption when the optimal sorption pH is close to neutral (sorption of metal cations by chelation) or the reciprocal alkaline solutions for desorbing metal anions (bound in acidic conditions by ion-exchange/electrostatic attraction). Alternatively, metal ions can be desorbed using strong chelating agents such as EDTA. In the present case, both the biopolymer and magnetic core can be very sensitive to acidic solutions: the crosslinking of chitosan prevents its dissolving at pH 1; however, a significant fraction of Fe_3O_4 may dissolve at pH below 1.5. For these reasons, acidic chelating solutions were chosen for the recovery of REEs from the loaded sorbent: thiourea

Table 6 Sorbent recycling: sorption capacity and sorption efficiency for five successive sorption/desorption cycles

Cycle	Nd		Dy		Yb	
	q_e (mg Nd g^{-1})	S. eff. (%)	q_e (mg Dy g^{-1})	S. eff. (%)	q_e (mg Yb g^{-1})	S. eff. (%)
Cycle I	47.4	100.0	49.3	100.0	50.1	100.0
Cycle II	46.2	97.6	47.9	97.3	48.5	96.7
Cycle III	45.7	96.4	47.5	96.4	48.0	95.7
Cycle IV	45.3	95.7	47.1	95.5	47.6	95.0
Cycle V	45.1	95.1	46.7	94.7	45.6	94.1

(acidified with a few drops of 0.2 M sulfuric acid solutions, i.e., pH 2–3) was used for metal desorption. Sorbent rinsing between each sorption and desorption step was performed with demineralized water. Table 6 reports the variation of sorption capacity and sorption yield at each sorption cycle. The sorption efficiency progressively decreases but at the firth cycle the variation does not exceed 6 %. The decrease may be attributed to a partial degradation of the sorbent and/or an incomplete desorption of the sorbed metal ions. However, the sorption performance remains quite good for allowing supplementary sorption/desorption cycles. Acidic thiourea solution is efficient at removing loaded REEs (by complexation and destabilization of ion-exchange interactions between the sorbent and metal cations) and recycling the spent sorbent.

Selective sorption

Both equilibrium and dynamic experiments show that the sorbent has very similar sorption properties for the three REEs belonging to different families (i.e., light, mild and heavy REEs); a selective separation of individual REEs appears difficult. A complementary experiment was performed on a binary REE solution containing equimolar concentrations of light REE [i.e., Nd(III): 0.23 mmol Nd L^{-1}; 59.5 mg Nd L^{-1}] and heavy REE [i.e., Yb(III): 0.25 mmol Yb L^{-1}; 53.8 mg Yb L^{-1}]. At metal-binding equilibrium, the sorption capacities reach 29.6 mg Yb g^{-1} (i.e., 0.17 mmol Yb g^{-1}) and 20.6 mg Nd g^{-1} (0.14 mmol Nd g^{-1}), respectively. In the solution, the molar ratio Yb(III)/Nd(III) was initially close to 1.087; after metal sorption, the molar ratio Yb(III)/Nd(III) in the sorbent increased to 1.21. A slight concentration effect in the sorbent was observed for Yb(III), while Nd(IIII) was enriched in the solution. However, these differences were not very marked and would have required numerous enrichment steps for achieving metal separation. The total sorption capacity was close to 50 mg metal g^{-1}: this means a value close to the maximum sorption capacities found for the binding of REEs (see Table 3; Fig. 3). As expected, the metal ions competed for the same reactive groups.

Actually, the effect of counter anions on metal sorption was not tested. Previous studies on other sorbents showed that the type of anion (chloride, nitrate and sulfate) present in the solution did not significantly affect the binding of La(III), Eu(III) and Yb(III) on *Pseudomonas aeruginosa* (Texier et al. 1999). On the contrary, Diniz and Volesky (Diniz and Volesky 2005b) observed a decrease in the La(III) sorption capacity in the presence sulfate anions compared to chloride and nitrate solutions on *Sargassum polycystum* (biomass). The complexation of La(III) with sulfate anions led to monovalent cations with a lower affinity for the biosorbent. The process used for preparing metal solutions (involving sulfuric acid dissolution of the salt) may thus induce a slight decrease in sorption properties.

Conclusion

The incorporation of a magnetic core (Fe_3O_4) in nano-based chitosan particles allows producing very small sorbent particles (a few tens of nm) that can be readily recovered by an external magnetic field: the particles are superparamagnetic. By chemical modification and grafting of DETA through immobilization on epichlorohydrin spacer arms, it is possible to introduce new reactive groups (such as supplementary amino

groups). The sorbent, whose binding performance increases with pH, has sorption capacities close to 47–50 mg metal g^{-1}, regardless of the type of REE (i.e., no change in sorption performance for light, mild and heavy REEs). The sorption isotherms are well fitted by the Langmuir equation. The small size of sorbent particles allows reducing the impact of resistance to intraparticle diffusion on the control of uptake kinetics, which is correctly fitted by the pseudo-second order rate equation. The thermodynamic parameters have been determined: the reaction is endothermic, spontaneous and controlled by entropic rather than enthalpic constraints. The randomness of the system increases with REE sorption (hydration water released from metal ions during metal sorption contributes to increased disorder). Metal desorption can be performed using acidic thiourea solutions: the sorption efficiency decreases by less than 6 % at the fifth cycle. In addition, the competitive sorption of REEs from binary Nd(III)/Yb(III) solutions shows that the sorbent slightly concentrates Yb(III), while Nd(III) is enriched in the residual solution. However, the selective separation of Nd(III) from Yb(III) is not sufficent for reaching full separation of REEs from different families (i.e., light from heavy metal ions).

These materials were initially tested with the objective of separating light, middle and heavy REEs. These results show that these sorbents are more appropriate for the unselective recovery of REEs from dilute solution (as an enriching pretreatment) in batch systems. More conventional processes [using other specific sorbents (Roosen et al. 2014) or chromatographic-like long columns with specific ligands for improving the selectivity of separation] should be used for the separation of the different metals in the REE family.

Acknowledgments This work was supported by the French Government through a fellowship granted to A.G. by the French Embassy in Egypt (Institut Français d'Egypte). Special dedication to the memory of Prof. Dr. Ahmed Donia.

References

Abdel-Rahman AAH, El Aassy IE, Ahmed FY, Hamza MF (2010) Studies on the uptake of rare earth elements on polyacrylamidoxime resins from natural concentrate leachate solutions. J Dispersion Sci Technol 31:1128–1135. doi:10.1080/01932690903224821

Abreu RD, Morais CA (2014) Study on separation of heavy rare earth elements by solvent extraction with organophosphorus acids and amine reagents. Miner Eng 61:82–87. doi:10.1016/j.mineng.2014.03.015

Aghayan H, Mahjoub AR, Khanchi AR (2013) Samarium and dysprosium removal using 11-molybdo-vanadophosphoric acid supported on Zr modified mesoporous silica SBA-15. Chem Eng J 225:509–519. doi:10.1016/j.cej.2013.03.092

Allouche F-N, Guibal E, Mameri N (2014) Preparation of a new chitosan-based material and its application for mercury sorption. Colloids Surf A 446:224–232. doi:10.1016/j.colsurfa.2014.01.025

Barron L, O'Toole M, Diamond D, Nesterenko PN, Paull B (2008) Separation of transition metals on a poly-iminodiacetic acid grafted polymeric resin column with post-column reaction detection utilising a paired emitter-detector diode system. J Chromatogr A 1213:31–36. doi:10.1016/j.chroma.2008.08.049

Cadogan EI, Lee C-H, Popuri SR, Lin H-Y (2014) Efficiencies of chitosan nanoparticles and crab shell particles in europium uptake from aqueous solutions through biosorption: synthesis and characterization. Int Biodeterior Biodegrad Part A 95:232–240. doi:10.1016/j.ibiod.2014.06.003

Cotton S (2006) Lanthanide and actinide chemistry. Wiley, Chichester

Das N, Das D (2013) Recovery of rare earth metals through biosorption: an overview. J Rare Earths 31:933–943. doi:10.1016/s1002-0721(12)60382-2

Diniz V, Volesky B (2005a) Biosorption of La, Eu and Yb using *Sargassum* biomass. Water Res 39:239–247. doi:10.1016/j.waters.2004.09.009

Diniz V, Volesky B (2005b) Effect of counterions on lanthanum biosorption by *Sargassum polycystum*. Water Res 39:2229–2236. doi:10.1016/j.watres.2005.04.004

Dubinin MM, Zaverina ED, Radushkevich LV (1947) Sorption and structure of active carbons. I. Adsorption of organic vapors. Zh Fiz Khim 21:1351–1362

El-Didamony H, Ali MM, Awwad NS, Fawzy MM, Attallah MF (2012) Treatment of phosphogypsum waste using suitable organic extractants. J Radioanal Nucl Chem 291:907–914. doi:10.1007/s10967-011-1547-3

Elwakeel KZ, Atia AA (2014) Uptake of U(VI) from aqueous media by magnetic Schiff's base chitosan composite. J Cleaner Prod 70:292–302. doi:10.1016/j.jclepro.2014.02.017

Elwakeel KZ, Atia AA, Donia AM (2009) Removal of Mo(VI) as oxoanions from aqueous solutions using chemically modified magnetic chitosan resins. Hydrometallurgy 97:21–28. doi:10.1016/j.hydromet.2008.12.009

Elwakeel KZ, Atia AA, Guibal E (2014) Fast removal of uranium from aqueous solutions using tetraethylenepentamine modified magnetic chitosan resin. Bioresour Technol 160:107–114. doi:10.1016/j.biortech.2014.01.037

Elyamani IS, Shabana EI (1985) Solvent-extraction of Lanthanum(III) from sulfuric-acid solutions by Primene JMT. J Less Common Met 105:255–261. doi:10.1016/0022-5088(85)90412-6

Foo KY, Hameed BH (2010) Insights into the modeling of adsorption isotherm systems. Chem Eng J 156:2–10. doi:10.1016/j.cej.2009.09.013

Freundlich HMF (1906) Uber die adsorption in lasungen. Z Phys Chem 57:385–470

Gao YH, Oshita K, Lee KH, Oshima M, Motomizu S (2002) Development of column-pretreatment chelating resins for matrix elimination/multi-element determination by inductively coupled plasma-mass spectrometry. Analyst 127:1713–1719. doi:10.1039/b208341h

Greenwood NN, Earnshaw A (1997) Chemistry of the elements, 2nd edn. Butterworth-Heinemann, Oxford

Guibal E (2004) Interactions of metal ions with chitosan-based sorbents: a review. Sep Purif Technol 38:43–74. doi:10.1016/j.seppur.2003.10.004

Hakim L, Sabarudin A, Oshima M, Motomizu S (2007) Synthesis of novel chitosan resin derivatized with serine diacetic acid moiety and its application to on-line collection/concentration of trace elements and their determination using inductively coupled plasma-atomic emission spectrometry. Anal Chim Acta 588:73–81. doi:10.1016/j.aca.2007.01.066

Hosomomi Y, Baba Y, Kubota F, Kamiya N, Goto M (2013) Biosorption of rare earth elements by *Escherichia coli*. J Chem Eng Jpn 46:450–454. doi:10.1252/jcej.13we031

Hu X-J et al (2011) Adsorption of chromium (VI) by ethylenediamine-modified cross-linked magnetic chitosan resin: isotherms, kinetics and thermodynamics. J Hazard Mater 185:306–314. doi:10.1016/j.jhazmat.2010.09.034

Innocenzi V, De Michelis I, Kopacek B, Veglio F (2014) Yttrium recovery from primary and secondary sources: a review of main hydrometallurgical processes. Waste Manage (Oxford) 34:1237–1250. doi:10.1016/j.wasman.2014.02.010

Jayakumar R, Prabaharan M, Reis RL, Mano JF (2005) Graft copolymerized chitosan—present status and applications. Carbohydr Polym 62:142–158. doi:10.1016/j.carbpol.2005.07.017

Koochaki-Mohammadpour SMA, Torab-Mostaedi M, Talebizadeh-Rafsanjani A, Naderi-Behdani F (2014) Adsorption isotherm, kinetic, thermodynamic, and desorption studies of lanthanum and dysprosium on oxidized multiwalled carbon nanotubes. J Dispers Sci Technol 35:244–254. doi:10.1080/01932691.2013.785361

Kozhevnikova NM, Tsybikova NL (2008) Sorption of neodymium(III) ions by natural mordenite-containing tuff. Russ J Appl Chem 81:42–45. doi:10.1134/s1070427208010102

Krishna PG, Gladis JM, Rao TP, Naidu GR (2005) Selective recognition of neodymium(III) using ion imprinted polymer particles. J Mol Recognit 18:109–116. doi:10.1002/jmr.720

Langmuir I (1918) The adsorption of gases on plane surfaces of glass, mica and platinum. J Amer Chem Soc 40:1361–1402

Lee GS, Uchikoshi M, Mimura K, Isshiki M (2010) Separation of major impurities Ce, Pr, Nd, Sm, Al, Ca, Fe, and Zn from La using bis(2-ethylhexyl)phosphoric acid (D2EHPA)-impregnated resin in a hydrochloric acid medium. Sep Purif Technol 71:186–191. doi:10.1016/j.seppur.2009.11.020

Lokshin EP, Ivanenko VI, Tareeva OA, Korneikov RI (2013) Sorption of rare earth elements of waste solution of leaching uranium. Russ J Appl Chem 86:450–452. doi:10.1134/s1070427213030269

Mahfouz MG, Galhoum AA, Gomaa NA, Abdel-Rehem SS, Atia AA, Vincent T, Guibal E (2015) Uranium extraction using magnetic nano-based particles of diethylenetriamine-functionalized chitosan: equilibrium and kinetic studies. Chem Eng J 262:198–209. doi:10.1016/j.cej.2014.09.061

Marcus Y (1997) Ion properties. Marcel Dekker Inc., New York

Martins TS, Isolani PC (2005) Rare earths: industrial and biological applications. Quim Nova 28:111–117. doi:10.1590/s0100-40422005000100020

Melnyk IV, Goncharyk VP, Kozhara LI, Yurchenko GR, Matkovsky AK, Zub YL, Alonso B (2012a) Sorption properties of porous spray-dried microspheres functionalized by phosphonic acid groups. Microporous Mesoporous Mater 153:171–177. doi:10.1016/j.micromeso.2011.12.027

Melnyk IV, Goncharyk VP, Stolyarchuk NV, Kozhara LI, Lunochkina AS, Alonso B, Zub YL (2012b) Dy(III) sorption from water solutions by mesoporous silicas functionalized with phosphonic acid groups. J Porous Mater 19:579–585. doi:10.1007/s10934-011-9508-3

Morf LS, Gloor R, Haag O, Haupt M, Skutan S, Di Lorenzo F, Boeni D (2013) Precious metals and rare earth elements in municipal solid waste—Sources and fate in a Swiss incineration plant. Waste Manage (Oxford) 33:634–644. doi:10.1016/j.wasman.2012.09.010

Namdeo M, Bajpai SK (2008) Chitosan-magnetite nanocomposites (CMNs) as magnetic carrier particles for removal of Fe(III) from aqueous solutions. Colloids Surf A 320:161–168. doi:10.1016/j.colsurfa.2008.01.053

Oliveira RC, Jouannin C, Guibal E, Garcia O Jr (2011) Samarium(III) and praseodymium(III) biosorption on *Sargassum* sp.: batch study. Proc Biochem 46:736–744. doi:10.1016/j.procbio.2010.11.021

Oliveira RC, Guibal E, Garcia O Jr (2012) Biosorption and desorption of lanthanum(III) and neodymium(III) in fixed-bed columns with *Sargassum* sp.: perspectives for separation of rare earth metals. Biotechnol Progr 28:715–722. doi:10.1002/btpr.1525

Oshita K, Takayanagi T, Oshima M, Motomizu S (2007) Adsorption behavior of cationic and anionic species on chitosan resins possessing amino acid moieties. Anal Sci 23:1431–1434. doi:10.2116/analsci.23.1431

Oshita K, Sabarudin A, Takayanagi T, Oshima M, Motomizu S (2009) Adsorption behavior of uranium(VI) and other ionic species on cross-linked chitosan resins modified with chelating moieties. Talanta 79:1031–1035. doi:10.1016/j.talanta.2009.03.035

Park H-J, Tavlarides LL (2010) Adsorption of neodymium(III) from aqueous solutions using a phosphorus functionalized adsorbent. Ind Eng Chem Res 49:12567–12575. doi:10.1021/ie100403b

Pearson RG (1966) Acids and bases. Science 151:172–177. doi:10.1126/science.151.3707.172

Qadeer R, Hanif J (1995) Adsorption of dysprosium ions on activated-charcoal from aqueous solutions. Carbon 33:215–220. doi:10.1016/0008-6223(94)00135-m

Qiu H, Lv L, Pan B, Zhang Q, Zhang W, Zhang Q (2009) Review: critical review in adsorption kinetic models. J Zhejiang Univ Sci A 10:716–724

Qu Y, Lian B (2013) Bioleaching of rare earth and radioactive elements from red mud using *Penicillium tricolor RM-10*.

Bioresour Technol 136:16–23. doi:10.1016/j.biortech.2013.03.070

Rabatho JP, Tongamp W, Takasaki Y, Haga K, Shibayama A (2013) Recovery of Nd and Dy from rare earth magnetic waste sludge by hydrometallurgical process. J Mater Cycles Waste Manage 15:171–178. doi:10.1007/s10163-012-0105-6

Rahmati A, Ghaemi A, Samadfam M (2012) Kinetic and thermodynamic studies of uranium(VI) adsorption using Amberlite IRA-910 resin. Ann Nucl Energy 39:42–48. doi:10.1016/j.anucene.2011.09.006

Ren Y, Abbood HA, He F, Peng H, Huang K (2013) Magnetic EDTA-modified chitosan/SiO_2/Fe_3O_4 adsorbent: preparation, characterization, and application in heavy metal adsorption. Chem Eng J 226:300–311. doi:10.1016/j.cej.2013.04.059

Repo E, Warchol JK, Bhatnagar A, Mudhoo A, Sillanpaa M (2013) Aminopolycarboxylic acid functionalized adsorbents for heavy metals removal from water. Water Res 47:4812–4832. doi:10.1016/j.watres.2013.06.020

Roosen J, Binnemans K (2014) Adsorption and chromatographic separation of rare earths with EDTA- and DTPA-functionalized chitosan biopolymers. J Mater Chem A 2:1530–1540. doi:10.1039/c3ta14622g

Roosen J, Spooren J, Binnemans K (2014) Adsorption performance of functionalized chitosan-silica hybrid materials toward rare earths. J Mater Chem A 2:19415–19426. doi:10.1039/c4ta04518a

Ruiz M, Sastre AM, Guibal E (2002a) Pd and Pt recovery using chitosan gel beads: II. Influence of chemical and physical modification on sorption properties. Sep Sci Technol 37:2385–2403

Ruiz MA, Sastre AM, Guibal E (2002b) Pd and Pt recovery using chitosan gel beads: I. Influence of drying process on diffusion properties. Sep Sci Technol 37:2143–2166

Russo P, Acierno D, Palomba M, Carotenuto G, Rosa R, Rizzuti A, Leonelli C (2012) Ultrafine magnetite nanopowder: synthesis, characterization, and preliminary use as filler of polymethylmethacrylate nanocomposites. J Nanotechnol 2012:8. doi:10.1155/2012/728326

Sapsford DJ, Bowell RJ, Geroni JN, Penman KM, Dey M (2012) Factors influencing the release rate of uranium, thorium, yttrium and rare earth elements from a low grade ore. Miner Eng 39:165–172. doi:10.1016/j.mineng.2012.08.002

Sui N, Huang K, Zhang C, Wang N, Wang F, Liu H (2013) Light, middle, and heavy rare-earth group separation: a new approach via a liquid-liquid-liquid three-phase system. Ind Eng Chem Res 52:5997–6008. doi:10.1021/ie4002553

Temkin VP (1940) Kinetics of ammonia synthesis on promoted iron catalysts. Acta Physiochim 12:217–222

Texier AC, Andres Y, Le Cloirec P (1999) Selective biosorption of lanthanide (La, Eu, Yb) ions by *Pseudomonas aeruginosa*. Environ Sci Technol 33:489–495. doi:10.1021/es9807744

Tunsu C, Ekberg C, Foreman M, Retegan T (2014) Studies on the solvent extraction of rare earth metals from fluorescent lamp waste using Cyanex 923. Solvent Extr Ion Exch 32:650–668. doi:10.1080/07366299.2014.925297

Vander Hoogerstraete T, Binnemans K (2014) Highly efficient separation of rare earths from nickel and cobalt by solvent extraction with the ionic liquid trihexyl (tetradecyl) phosphonium nitrate: a process relevant to the recycling of rare earths from permanent magnets and nickel metal hydride batteries. Green Chem 16:1594–1606. doi:10.1039/c3gc41577e

Vijayaraghavan K, Sathishkumar M, Balasubramanian R (2011) Interaction of rare earth elements with a brown marine alga in multi-component solutions. Desalination 265:54–59. doi:10.1016/j.desal.2010.07.030

Vlachou A, Symeopoulos BD, Koutinas AA (2009) A comparative study of neodymium sorption by yeast cells. Radiochim Acta 97:437–441. doi:10.1524/ract.2009.1632

Wan Ngah WS, Endud CS, Mayanar R (2002) Removal of copper(II) ions from aqueous solution onto chitosan and cross-linked chitosan beads. React Funct Polym 50:181–190

Wang J-S, Peng R-T, Yang J-H, Liu Y-C, Hu X-J (2011) Preparation of ethylenediamine-modified magnetic chitosan complex for adsorption of uranyl ions. Carbohydr Polym 84:1169–1175. doi:10.1016/j.carbpol.2011.01.007

Wu D, Zhang L, Wang L, Zhu B, Fan L (2011) Adsorption of lanthanum by magnetic alginate-chitosan gel beads. J Chem Technol Biotechnol 86:345–352. doi:10.1002/jctb.2522

Xie F, Zhang TA, Dreisinger D, Doyle F (2014) A critical review on solvent extraction of rare earths from aqueous solutions. Miner Eng 56:10–28. doi:10.1016/j.mineng.2013.10.021

Xiong C, Zheng Z (2010) Evaluation of D113 cation exchange resin for the removal of Eu(III) from aqueous solution. J Rare Earths 28:862–867. doi:10.1016/s1002-0721(09)60231-3

Xiong C, Yao C, Wang Y (2006) Sorption behaviour and mechanism of ytterbium(III) on imino-diacetic acid resin. Hydrometallurgy 82:190–194. doi:10.1016/j.hydromet.2006.03.012

Xu T, Peng H (2009) Formation cause, composition analysis and comprehensive utilization of rare earth solid wastes. J Rare Earths 27:1096–1102. doi:10.1016/s1002-0721(08)60394-4

Xu J, Chen M, Zhang C, Yi Z (2013) Adsorption of uranium(VI) from aqueous solution by diethylenetriamine-functionalized magnetic chitosan. J Radioanal Nucl Chem 298:1375–1383. doi:10.1007/s10967-013-2571-2

Xue X, Wang J, Mei L, Wang Z, Qi K, Yang B (2013) Recognition and enrichment specificity of Fe_3O_4 magnetic nanoparticles surface modified by chitosan and *Staphylococcus aureus* enterotoxins A antiserum. Colloids Surf B 103:107–113. doi:10.1016/j.colsurfb.2012.10.013

Yoon H-S et al (2014) Leaching kinetics of neodymium in sulfuric acid of rare earth elements (REE) slag concentrated by pyrometallurgy from magnetite ore. Korean J Chem Eng 31:1766–1772. doi:10.1007/s11814-014-0078-3

Zhang S-G, Yang M, Liu H, Pan D-A, Tian J-J (2013) Recovery of waste rare earth fluorescent powders by two steps acid leaching. Rare Met 32:609–615. doi:10.1007/s12598-013-0170-6

Zhao F, Repo E, Yin D, Sillanpaa MET (2013) Adsorption of Cd(II) and Pb(II) by a novel EGTA-modified chitosan material: kinetics and isotherms. J Colloid Interface Sci 409:174–182. doi:10.1016/j.jcis.2013.07.062

Zhao FP, Repo E, Sillanpaa M, Meng Y, Yin DL, Tang WZ (2015) Green synthesis of magnetic EDTA- and/or DTPA-cross-linked chitosan adsorbents for highly efficient removal of metals. Ind Eng Chem Res 54:1271–1281. doi:10.1021/ie503874x

Zhou J, Duan W, Zhou X, Zhang C (2007) Application of annular centrifugal contactors in the extraction flowsheet for producing high purity yttrium. Hydrometallurgy 85:154–162. doi:10.1016/j.hydromet.2006.08.010

Zhou L, Xu J, Liang X, Liu Z (2010) Adsorption of platinum(IV) and palladium(II) from aqueous solution by magnetic cross-linking chitosan nanoparticles modified with ethylenediamine. J Hazard Mater 182:518–524. doi:10.1016/j.jhazmat.2010.06.062